Homotopy based solutions of the Navier–Stokes equations for a porous channel with orthogonally moving walls

Hang Xu,[1,a)] Zhi-Liang Lin,[1] Shi-Jun Liao,[1,b)] Jie-Zhi Wu,[2,c)] and Joseph Majdalani[2,d)]
[1]*State Key Lab of Ocean Engineering, School of Naval Architecture, Ocean and Civil Engineering, Shanghai Jiao Tong University, Shanghai 200240, China*
[2]*University of Tennessee Space Institute, Tullahoma, Tennessee 37388, USA*

(Received 5 May 2009; accepted 24 February 2010; published online 4 May 2010)

This paper focuses on the theoretical treatment of the laminar, incompressible, and time-dependent flow of a viscous fluid in a porous channel with orthogonally moving walls. Assuming uniform injection or suction at the porous walls, two cases are considered for which the opposing walls undergo either uniform or nonuniform motions. For the first case, we follow Dauenhauer and Majdalani [Phys. Fluids **15**, 1485 (2003)] by taking the wall expansion ratio α to be time invariant and then proceed to reduce the Navier–Stokes equations into a fourth order ordinary differential equation with four boundary conditions. Using the homotopy analysis method (HAM), an optimized analytical procedure is developed that enables us to obtain highly accurate series approximations for each of the multiple solutions associated with this problem. By exploring wide ranges of the control parameters, our procedure allows us to identify dual or triple solutions that correspond to those reported by Zaturska *et al.* [Fluid Dyn. Res. **4**, 151 (1988)]. Specifically, two new profiles are captured that are complementary to the type I solutions explored by Dauenhauer and Majdalani. In comparison to the type I motion, the so-called types II and III profiles involve steeper flow turning streamline curvatures and internal flow recirculation. The second and more general case that we consider allows the wall expansion ratio to vary with time. Under this assumption, the Navier–Stokes equations are transformed into an exact nonlinear partial differential equation that is solved analytically using the HAM procedure. In the process, both algebraic and exponential models are considered to describe the evolution of $\alpha(t)$ from an initial α_0 to a final state α_1. In either case, we find the time-dependent solutions to decay very rapidly to the extent of recovering the steady state behavior associated with the use of a constant wall expansion ratio. We then conclude that the time-dependent variation of the wall expansion ratio plays a secondary role that may be justifiably ignored. © *2010 American Institute of Physics*. [doi:10.1063/1.3392770]

I. INTRODUCTION

Studies of laminar motions through porous channels continue to receive attention in the fluid and mathematical communities due to their interesting connections with a variety of applications. These include binary gas diffusion, filtration, ablation cooling, surface sublimation, and the modeling of air circulation in the respiratory system. Berman[1] initiated the analysis of the steady laminar flow of a viscous incompressible fluid in a two-dimensional porous channel with uniform injection or suction. With the assumption that the transverse velocity component remained independent of the streamwise coordinate, Berman reduced the Navier–Stokes equations to a nonlinear ordinary differential equation (ODE) with appropriate boundary conditions. He then proceeded to construct an asymptotic approximation for a small Reynolds number R using a regular perturbation scheme.

Extensions to Berman's solution[1] followed shortly thereafter. For example, Terrill[2] obtained series solutions for both small and large values of R that compared favorably with the numerical solutions to this problem. Using the method of averages, Morduchow[3] presented a solution which covered the entire injection range. Later, White *et al.*[4] derived a power series expansion that appeared to retain its validity for arbitrary R. However, their solution required the numerical calculation of numerous power series coefficients that could not be tied recursively. Other studies devoted to the analysis of the symmetrically porous channel flow problem were reported by a diverse group of investigators. To list a few, one may enumerate Sellars,[5] Shrestha,[6] Robinson,[7] Skalak and Wang,[8] Brady,[9] Durlofsky and Brady,[10] Zaturska *et al.*,[11] Taylor,[12] and Yuan.[13]

Following this string of investigations, at least two prominent categories of flow variations emerged, thus creating new tracks for sustained research inquiry. The attendant motions incorporated either asymmetries in the mean flow configuration or translational movement of the boundaries. The class of asymmetrical flows could be achieved, for example, by imposing different wall suction rates, as in the case examined by Proudman[14] under steady laminar conditions and large Reynolds numbers. The flow analog at small

[a)]Electronic mail: hangxu@sjtu.edu.cn.
[b)]Electronic mail: sjliao@sjtu.edu.cn.
[c)]Electronic mail: jzwu@coe.pku.edu.cn. Permanent address: State Key Laboratory for Turbulence and Complex System, Peking University, Beijing 100871, China.
[d)]Author to whom correspondence should be addressed. Electronic mail: maji@utsi.edu.

R was equally investigated by Terrill and Shrestha.[15] Shrestha and Terrill[16] also provided accurate series solutions for large wall injection using the method of inner and outer expansions.

The problem comprising moving boundaries appears to have been initiated by Brady and Acrivos.[17] These researchers obtained an exact solution to the Navier–Stokes equations for the flow in a channel with an accelerating surface velocity. Their work was revisited in the context of a moving porous wall by Watson *et al.*[18] Watson *et al.*[19] then combined asymmetry with wall movement in their analysis of the two-dimensional porous channel. Along similar lines, Dauenhauer and Majdalani[20] presented a new similarity solution for the laminar, incompressible, and time-dependent Navier–Stokes equations in the context of a porous channel with expanding or contracting walls. Assuming a constant (or quasiconstant) wall expansion ratio α, they reduced the Navier–Stokes equations into a self-similar ODE that could be solved numerically. Their approach employed Runge–Kutta integration coupled with a rapidly converging shooting technique to cover a modest range of R and wall expansion ratios. Asymptotic solutions for the problem were later provided by Majdalani and Zhou[21] for moderate-to-large R and by Majdalani *et al.*[22] for small R. The solution in the context of rocket propulsion is also discussed by Zhou and Majdalani.[23] As for the stability of these flows, this vital topic was originally addressed by Zaturska *et al.*,[11] although several illuminating investigations have been carried out by MacGillivray and Lu,[24] Lu,[25] and Cox and King,[26] to name a few.

In this paper, we revisit the porous channel flow problem with regressing walls and solve it using a series expansion approach known as the homotopy analysis method (HAM). This method was developed by Liao[27–31] as an improvement over the Adomian decomposition framework. In this context, it was developed for the purpose of obtaining series solutions to strongly nonlinear differential equations. Its implementation involves the introduction of an embedding parameter q that permits converting the nonlinear governing equation into a linear equation for $q=0$. As q is increased, homotopy ensures that the original nonlinear equation is recovered in the limit of $q \to 1$. As discussed in several articles,[32–39] HAM has been shown to exhibit several distinct advantages over other asymptotic techniques. For example, HAM provides a convenient control parameter $\hbar$ that helps to ensure series convergence.[28–31] HAM can also be applied with equal level of ease to nonlinear ODEs and partial differential equations (PDEs). This makes it an ideal approach for handling the Dauenhauer–Majdalani PDE considered in this study.

To set the stage, we first revisit the exact similarity equation rendered by Dauenhauer and Majdalani[20] for the porous channel flow. Given that these investigators were mainly interested in the type I injection and suction solutions that pertained to their application, our analysis will seek to unravel not only the classical type I, but other possible solutions that have been classified as types II and III by Zaturska *et al.*[11] To this end, an optimal HAM-based approach will be developed with the capability of capturing multiple solutions. This will enable us to obtain multiple solutions under suction dominated conditions that have not been discussed before. By way of verification, our series approximations will be shown to agree substantially well with the numerically integrated solution described by Dauenhauer and Majdalani.[20]

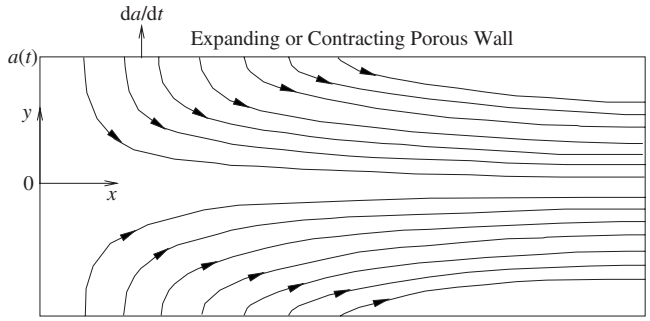

FIG. 1. Coordinate system and characteristic streamlines used to describe the fluid flow pattern.

In seeking further generalization, the Dauenhauer–Majdalani model[20] will be extended to the case for which the wall expansion ratio α is no longer constant, but rather a time-dependent variable that transitions from α_0 to α_1. The corresponding similarity equation is readily turned into a nonlinear PDE that can be solved analytically. While it would be helpful to consider a case for which the channel half-height a varies from an initial value a_0 to a final a_1, such a situation may be considered to be a special case of the model used here. For example, knowing the initial and final heights, one can calculate the average expansion ratio using, for example, $\dot{a} \approx (a_1 - a_0)/(t_1 - t_0)$, where $t_1 - t_0$ represents the time for expansion. Then knowing $\dot{a}$, one can calculate $\alpha_0 = \dot{a}a_0/\nu$ and $\alpha_1 = \dot{a}a_1/\nu$, where ν is the kinematic viscosity.

The basic equations for the channel flow problem with both constant and time-dependent wall expansion ratios are described in Sec. II. In Sec. III, a conventional HAM approach is implemented for the purpose of capturing one of the multiple solutions. This is followed by the presentation of an optimal HAM-based approach that can be used to identify any number of solutions: single, dual, or triple solutions for the case of a constant wall expansion ratio. Therein, results are described and verified through comparisons to the numerical results obtained from the use of the Dauenhauer–Majdalani shooting approach.[20] In Sec. IV, a HAM-based approach is advanced for the case of a time-dependent wall expansion ratio. Finally, closing remarks and conclusions are given in Sec. V.

II. MATHEMATICAL DESCRIPTION

A. Basic equations

As shown in Fig. 1, the flow to be studied takes place in a two-dimensional rectangular channel bounded by porous walls at $y = \pm a$. The walls of the channel undergo either uniform or nonuniform expansion or contraction in the transverse direction. Through the two opposing walls fluid is uniformly injected or extracted at a constant speed v_w. The gov-

erning equations describing the unsteady flow of an incompressible fluid for mass and momentum conservation are

$$\frac{\partial u}{\partial x}+\frac{\partial v}{\partial y}=0, \tag{1}$$

$$\frac{\partial u}{\partial t}+u\frac{\partial u}{\partial x}+v\frac{\partial u}{\partial y}=-\frac{1}{\rho}\frac{\partial p}{\partial x}+\nu\left(\frac{\partial^2 u}{\partial x^2}+\frac{\partial^2 u}{\partial y^2}\right), \tag{2}$$

$$\frac{\partial v}{\partial t}+u\frac{\partial v}{\partial x}+v\frac{\partial v}{\partial y}=-\frac{1}{\rho}\frac{\partial p}{\partial y}+\nu\left(\frac{\partial^2 v}{\partial x^2}+\frac{\partial^2 v}{\partial y^2}\right). \tag{3}$$

These are subject to the following boundary conditions:

$$u=0, \quad v=-v_w; \quad y=a(t), \tag{4}$$

$$\frac{\partial u}{\partial y}=0, \quad v=0; \quad y=0, \tag{5}$$

$$u=0, \quad v=0; \quad x=0, \tag{6}$$

where Cartesian coordinates (x,y) that are fixed in space are taken, with the x-axis extending along the length of the channel and the y-axis in the wall-normal direction. Here u and v denote the velocity components along x- and y-axes, and ρ, p, ν, t, and v_w correspond to the dimensional density, pressure, kinematic viscosity, time, and (crossflow) injection velocity at the wall. Note that Eqs. (4)–(6) are written in the upper half-domain $(y\geq 0)$, thus taking into account symmetry with respect to the midsection plane while assuming an odd function for the wall normal velocity v and an even function for the axial velocity u.

Using ψ to denote a stream function such that $u=\partial\psi/\partial y$ and $v=-\partial\psi/\partial x$, the continuity equation is automatically satisfied and the vorticity transport equation is readily obtained by taking the curl of the momentum equation. One gets

$$\frac{\partial \zeta}{\partial t}+u\frac{\partial \zeta}{\partial x}+v\frac{\partial \zeta}{\partial y}=\nu\left(\frac{\partial^2 \zeta}{\partial x^2}+\frac{\partial^2 \zeta}{\partial y^2}\right), \tag{7}$$

where

$$\zeta=\frac{\partial v}{\partial x}-\frac{\partial u}{\partial y}=-\nabla^2\psi. \tag{8}$$

Substituting the dual transformations[20]

$$\psi=(\nu x/a)F(\eta,t), \quad \eta=y/a \tag{9}$$

into the vorticity transportation equation gives

$$[F_{\eta\eta\eta}+FF_{\eta\eta}+F_\eta(2\alpha-F_\eta)+\alpha\eta F_{\eta\eta}-(a^2/\nu)F_{\eta t}]_\eta=0, \tag{10}$$

which is subject to the four classical boundary conditions

$$\begin{cases}\eta=0: & F=0, \quad F_{\eta\eta}=0,\\ \eta=1: & F=R, \quad F_\eta=0.\end{cases} \tag{11}$$

Equation (10) describes the unsteady flow of an incompressible fluid in a porous channel. It is presented by White[40] as one of the new exact Navier–Stokes solutions attributed to Dauenhauer and Majdalani.[20] Here,

$$\alpha=\dot{a}a/\nu \tag{12}$$

is the wall expansion ratio in which a and $\dot{a}$ represent the half-height of the channel and its expansion speed; as before, ν is the kinematic viscosity and so $R=v_w a/\nu=A\alpha$ defines the crossflow Reynolds number, with A being the injection coefficient. Note that according to our sign convention, a positive R refers to injection conditions. More detail is given by Dauenhauer and Majdalani[20] where these steps are systematically developed.

B. Equation for uniform wall expansion

When the wall expansion ratio α is constant in time, the function F becomes dependent on η and α instead of (η,t). One can put $F_{\eta t}=0$ and write

$$\alpha=\dot{a}a/\nu=\dot{a}_0 a_0/\nu, \tag{13}$$

where a_0 and $\dot{a}_0$ are the initial channel height and expansion rate, respectively. Integrating Eq. (13) with respect to t yields

$$a/a_0=(1+2\nu\alpha t a_0^{-2})^{1/2}. \tag{14}$$

Moreover, given a constant injection coefficient A, one can put

$$\dot{a}/\dot{a}_0=v_w(t)/v_w(0)=(1+2\nu\alpha t a_0^{-2})^{-1/2}. \tag{15}$$

As shown by Dauenhauer and Majdalani,[20] an exact self-similarity equation emerges for Berman's main characteristic function F. After some algebra, one retrieves

$$F_{\eta\eta\eta\eta}+FF_{\eta\eta\eta}+F_{\eta\eta}(3\alpha-F_\eta)+\alpha\eta F_{\eta\eta\eta}=0, \tag{16}$$

with

$$\eta=0: \quad F=0, \quad F_{\eta\eta}=0; \quad \eta=1: \quad F=R, \quad F_\eta=0, \tag{17}$$

where F denotes a sole function of η. For more detail on the mathematical foundations of Eqs. (16) and (17), the reader is referred to Dauenhauer and Majdalani.[20]

C. Equation for nonuniform wall expansion

Another practical setting corresponds to the case for which the wall expansion ratio α is not restricted to a constant, but is rather permitted to vary as a function of t, namely, from α_0 to α_1. Letting

$$\beta(t)=\frac{a^2}{\nu}, \tag{18}$$

it follows that

$$\alpha(t)=\dot{a}a/\nu=\tfrac{1}{2}\beta_t(t). \tag{19}$$

Then taking into account Eq. (12), we can put

$$\alpha_0(t)=\alpha(0)=\dot{a}_0 a_0/\nu=\tfrac{1}{2}\beta_t(0). \tag{20}$$

If we now consider the hypothetical case for which the injection coefficient A is inversely proportional to $\alpha(t)$, Eq. (10) can be reduced to

$$F_{\eta\eta\eta\eta}+\alpha(t)(\eta F_{\eta\eta\eta}+3F_{\eta\eta})+FF_{\eta\eta\eta}-F_{\eta}F_{\eta\eta}-\beta(t)F_{\eta\eta t}=0, \tag{21}$$

where $F=F(\eta,t)$. This PDE is subject to the same fundamental boundary conditions delineated in Eq. (17). Its formulation constitutes another exact reduction of the Navier–Stokes equations that will be discussed in Sec. IV.

III. SOLUTIONS FOR CONSTANT EXPANSION RATIOS

A. Conventional HAM approach

In this section, we provide an accurate analytical approximation to Eq. (16). With the help of HAM, the explicit approximations for $F(\eta)$ can be specified as

$$F(\eta)=\sum_{m=0}^{M}\phi_m(\eta)=\sum_{m=0}^{M}\sum_{i=0}^{4m+4}\lambda_i^m a_i^m \eta^i, \tag{22}$$

where $\phi_m(\eta)$ is the so-called mth-order homotopy derivative, defined in the Appendix by Eq. (A13), and the coefficients a_i^m are given by

$$a_1^m=\chi_m\lambda_1^{m-1}a_1^{m-1}+C_m^1, \tag{23}$$

$$a_3^m=\chi_m\lambda_3^{m-1}a_3^{m-1}+C_m^3, \tag{24}$$

$$a_i^m=\lambda_i^{m-1}a_i^{m-1}+\frac{\hbar(e_{i-4}^{m-1}+3\alpha c_{i-4}^{m-1}+\chi_{i-3}d_{i-5}^{m-1}+\Upsilon_{i-4}^m+\Omega_{i-4}^m)}{i(i-1)(i-2)(i-3)} \tag{25}$$

for $3<i\leq 4m+3$, in which

$$b_i^m=(i+1)\lambda_{i+1}^m a_{i+1}^m, \tag{26}$$

$$c_i^m=(i+2)(i+1)\lambda_{i+2}^m a_{i+2}^m, \tag{27}$$

$$d_i^m=(i+3)(i+2)(i+1)\lambda_{i+3}^m a_{i+3}^m, \tag{28}$$

$$e_i^m=(i+4)(i+3)(i+2)(i+1)\lambda_{i+4}^m a_{i+4}^m, \tag{29}$$

$$\Upsilon_i^m=\sum_{k=0}^{m-1}\sum_{r=\max\{0,i-4m+4k\}}^{\max\{4k+4,i\}}\lambda_r^k a_r^k b_{i-r}^{m-k-1}, \tag{30}$$

$$\Omega_i^m=\sum_{k=0}^{m-1}\sum_{r=\max\{0,i-4m+4k\}}^{\max\{4k+4,i\}}b_r^k c_{i-r}^{m-k-1}, \tag{31}$$

$$C_0^m=C_2^m=0, \tag{32}$$

$$C_3^m=\frac{\hbar}{2}\sum_{i=0}^{4m+4}\frac{e_{i-4}^{m-1}+3\alpha c_{i-4}^{m-1}+\chi_{i-3}d_{i-5}^{m-1}+\Upsilon_{i-4}^m+\Omega_{i-4}^m}{i(i-1)(i-2)(i-3)}-\frac{\hbar}{2}\sum_{i=0}^{4m+4}\frac{e_{i-3}^{m-1}+3\alpha c_{i-3}^{m-1}+\chi_{i-2}d_{i-4}^{m-1}+\Upsilon_{i-3}^m+\Omega_{i-3}^m}{i(i-1)(i-2)}, \tag{33}$$

$$C_1^m=-\sum_{i=0}^{4m+4}\frac{e_{i-4}^{m-1}+3\alpha c_{i-4}^{m-1}+\chi_{i-3}d_{i-5}^{m-1}+\Upsilon_{i-4}^m+\Omega_{i-4}^m}{i(i-1)(i-2)(i-3)}-C_3^m, \tag{34}$$

$$\chi_m=\begin{cases}0, m=1,\\ 1, m>1,\end{cases} \tag{35}$$

and

$$\lambda_i^m=\begin{cases}1, & 1\leq i\leq 4m+3,\\ 0, & i<1 \text{ or } i>4m+3.\end{cases} \tag{36}$$

Using the initial guess function given by

$$\phi_0(\eta,t)=\tfrac{1}{2}R\ \ \eta(3-\eta^2), \tag{37}$$

the first four coefficients are found to be

$$a_1^0=\tfrac{3}{2}R,\quad a_2^0=0,\quad a_3^0=-\tfrac{1}{2}R,\quad a_4^0=0. \tag{38}$$

At this juncture, the explicit HAM series coefficients are fully determined. Other flow variables such as the velocity, pressure, and vorticity may be readily evaluated from their basic definitions. For example, the vorticity ζ may be retrieved from Eq. (8), viz.,

$$\zeta=-\nabla^2\psi=\frac{\partial v}{\partial x}-\frac{\partial u}{\partial y}=-\nu x a^{-3}F_{\eta\eta}. \tag{39}$$

Other variables are omitted here for the sake of brevity. It may be worth remarking that the convergence of the HAM approximations is guaranteed when the linear operator $\mathcal{L}$, the initial guess $\phi_0(\eta)$, and the values of the convergence-control parameter $\hbar$ are obtained in accordance with pre-established rules.[28,29] Usually, $\mathcal{L}$ and $\phi_0(\eta)$ are constructed based on the solution expression consistent with the nonlinear behavior associated with the problem at hand. In this first section, we use $\hbar=-1$. In a later section, we confirm that series convergence is guaranteed for $\hbar\in[-\frac{3}{2},-\frac{2}{3}]$, albeit not limited to this range exclusively.

In order to test the accuracy of our traditional HAM series approximations with $\hbar=-1$, we compare in Figs. 2(a) and 2(b) the HAM solution for the axial velocity, given by $F'(\eta)/R$, to the numerical results of Eq. (16). The corresponding curves are evaluated for $R=\pm 5$ and values of α ranging from -20 to 5. Clearly, a uniformly consistent agreement with numerics is realized owing, in large part, to the ability of the HAM approximation to capture the true, nonlinear behavior of the solution in the limit of an infinite series.

For the suction driven channel with no wall motion, Zaturska *et al.*[11] showed that one symmetric solution exists for $R\in[-12.165,0]$ and three symmetric solutions emerge when $R\in[-\infty,-12.165]$. In much the same way, the search for multiple solutions will have to be influenced by both R and α, thus requiring a separate mathematical treatment, as first explained by Dauenhauer and Majdalani.[20] This treatment will be carried out in Sec. III B. In the interim, the numerical technique used by Dauenhauer and Majdalani[20] will be used to study the emergence of solution multiplicity in suitable ranges of α and R. This is evident in Fig. 3 where

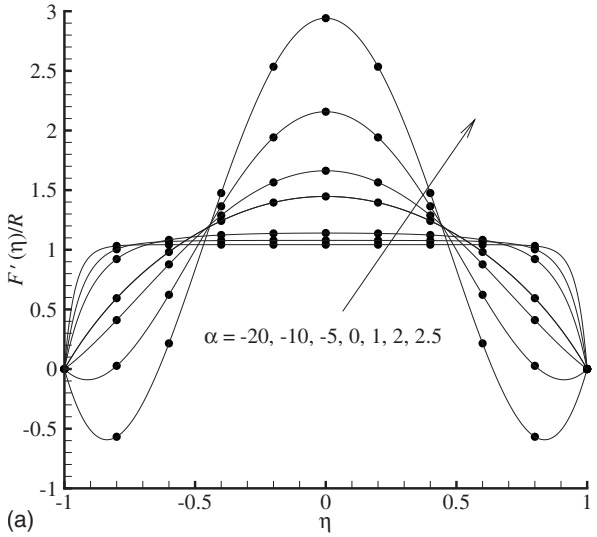

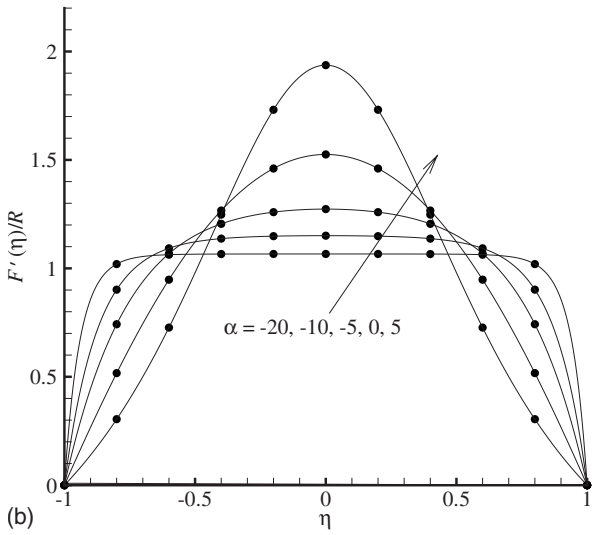

FIG. 2. Comparison between HAM-Padé approximations (circles) and numerical results (solid lines) for (a) $R=-5$ and (b) $R=5$ over some values of α.

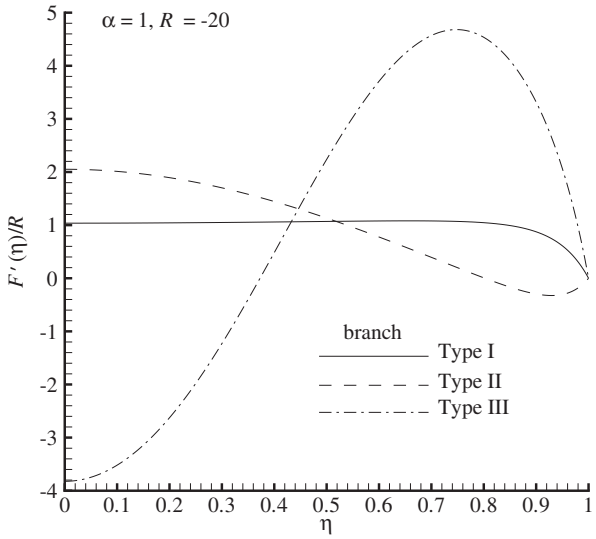

FIG. 3. Three solutions for $F'(\eta)/R$ at $\alpha=1$ and $R=-20$.

one particular case is considered (e.g., $\alpha=1$ and $R=-20$) for which three solution branches are seen to coexist. Using the conventional HAM approach, only type I can be predicted, although three types can be projected numerically. This apparent deficiency prompts us to modify the conventional HAM approach to the extent of granting it more generality. As we describe in Sec. III B, the extension will enable us to capture, using analytical series approximations, the three types of mean flow motions that are discussed by Zaturska *et al.*[11] in the case of a nonexpanding wall.

B. Optimal HAM approach for multiple solutions

In what follows, we describe the mathematical steps needed to mold the HAM to the porous channel flow problem with a constant expansion ratio α. We thus consider the steady PDE given by Eq. (16) and focus on its multiple solutions.

Note that there exist dual or even triple solutions for some values of R and α. In general, multiple solutions can be elusive even by numerical methods. Here, we provide an analytical framework that enables us to capture these multiple solutions. First, we introduce the transformation

$$F(\eta) = RS(\eta), \tag{40}$$

and so, the original equation becomes

$$S''' + \alpha(\eta S''' + 3S'') + R(SS''' - S'S'') = 0, \tag{41}$$

subject to the boundary conditions

$$S(0) = 0, \quad S''(0) = 0, \quad S(1) = 1, \quad S'(1) = 0, \tag{42}$$

where the prime denotes a derivative with respect to η. To help identify the multiple solutions that accompany different R and α, we define $F'(0)=R\,\gamma$, where

$$\gamma = S'(0). \tag{43}$$

Our strategy is guided by the shooting method described earlier.[20] Instead of using the original boundary conditions (42), we first apply HAM to secure analytical approximations for Eq. (41) using an initial value for $S'(0)$ at the lower end of the domain. We hence take

$$S(0) = 0, \quad S'(0) = \gamma, \quad S''(0) = 0, \quad S(1) = 1, \tag{44}$$

where γ is not known initially. At the conclusion of the analysis, γ may be determined from the actual boundary condition that must be observed at the upper end of the domain, specifically

$$S'(1) = 0. \tag{45}$$

At this juncture, the form of the analytical solutions to Eqs. (41) and (44) must be posited in terms of suitable functions. Given that Eq. (41) is defined over a finite domain $\eta \in [0,1]$, it is proper to express $S(\eta)$ in a power series of η. Besides, using Eq. (41) and the boundary conditions $S(0)=0$ and $S_{\eta\eta}(0)=0$, it can be shown that

$$\left.\frac{d^{2k}S}{d\eta^{2k}}\right|_{\eta=0}=0 \quad \text{when} \quad k=1,2,3,\ldots. \tag{46}$$

Thus, $S(\eta)$ may be expressed as

$$S(\eta)=\sum_{m=0}^{+\infty} B_m \eta^{2m+1}, \tag{47}$$

where the undetermined coefficient B_m is dependent on α. Equation (47) defines what is often referred to as the solution expression for $S(\eta)$. According to the homotopy-based approach, one needs to introduce an initial guess function of the form prescribed by Eq. (47) that still satisfies the problem's boundary conditions. For this reason, we choose, for the case of a constant wall expansion ratio, the following odd polynomial:

$$S_0(\eta)=A_0\eta+A_1\eta^3+A_2\eta^5. \tag{48}$$

This initial guess function may be readily made to satisfy the conditions given by Eqs. (44) and (45). The result is

$$A_0=\gamma, \quad A_1=\tfrac{5}{2}-2\gamma, \quad A_2=\gamma-\tfrac{3}{2}, \tag{49}$$

whence

$$S_0(\eta)=\gamma\eta+\left(\tfrac{5}{2}-2\gamma\right)\eta^3+\left(\gamma-\tfrac{3}{2}\right)\eta^5. \tag{50}$$

As with perturbation and traditional nonperturbation methods, HAM transforms a nonlinear problem into an infinite number of linear subproblems. Additionally, HAM provides greater freedom in selecting different base functions that serve to approximate solutions more efficiently. Equally importantly, perhaps, HAM provides the means to ensure the convergence of ensuing series solutions. This is accomplished through the use of the convergence-control parameter $\hbar$. By way of illustration, we note that, even for the nonlinear ODE, Eq. (41), it is not convenient to employ its entire linear part $\mathcal{L}=S'''+\alpha(\eta S''+3S')$ as the linear operator. Otherwise, the $\mathcal{L}=0$ solution would contain the error function $\mathrm{erf}(\eta)$; it would then become exceedingly difficult to retrieve higher-order approximations. This obstacle can be overcome by selecting an auxiliary operator of equal order, in this case, of fourth order, such as

$$\mathcal{L}\Phi=\frac{d^4\Phi}{d\eta^4}. \tag{51}$$

This operator has the property

$$\mathcal{L}(C_0+C_1\eta+C_2\eta^2+C_3\eta^3)=0, \tag{52}$$

where (C_0,C_1,C_2,C_3) are integral constants. This linear approximation is sufficient to satisfy the rule of solution expression, Eq. (47). It should be noted that the solution for $S(\eta)$, where $\eta\in[0,1]$, represents a mapping operation of $S:[0,1]\mapsto(-\infty,+\infty)$. Instead of solving Eq. (41) directly, we undergo continuous mapping according to

$$\Phi(\eta;q):[0,1]\times[0,1]\mapsto(-\infty,+\infty), \tag{53}$$

where

$$\Phi(\eta;0)=S_0(\eta), \quad \Phi(\eta;1)=S(\eta). \tag{54}$$

The mapping operation follows from the zeroth-order deformation equation

$$(1-q)\mathcal{L}[\Phi(\eta;q)-S_0(\eta)]=q\hbar\mathcal{N}[\Phi(\eta;q)], \tag{55}$$

which is subject to

$$\Phi(0;q)=0, \quad \left.\frac{\partial\Phi(\eta;q)}{\partial\eta}\right|_{\eta=0}=\gamma, \quad \left.\frac{\partial^2\Phi(\eta;q)}{\partial\eta^2}\right|_{\eta=0}=0, \quad \Phi(1;q)=1. \tag{56}$$

On the one hand, $q\in[0,1]$ denotes the embedment parameter mentioned before, while $\hbar$ alludes to the auxiliary parameter known as the convergence-control parameter.[27] On the other hand, $\mathcal{L}$ and $\mathcal{N}$ refer to the linear and nonlinear operators based on Eqs. (51) and (41), respectively. The latter is defined by

$$\mathcal{N}[\Phi(\eta;q)]=\frac{\partial^4\Phi}{\partial\eta^4}+\alpha\left(\eta\frac{\partial^3\Phi}{\partial\eta^3}+3\frac{\partial^2\Phi}{\partial\eta^2}\right)+R\left(\Phi\frac{\partial^3\Phi}{\partial\eta^3}-\frac{\partial\Phi}{\partial\eta}\frac{\partial^2\Phi}{\partial\eta^2}\right). \tag{57}$$

To make further headway, one may evaluate Eq. (55) at both ends of its limiting expressions to deduce

$$\begin{cases} q=0: & \mathcal{L}[\Phi(\eta;0)-S_0(\eta)]=0, \\ q=1: & \mathcal{N}[\Phi(\eta;1)]=0; \quad \forall\,\hbar\neq 0. \end{cases} \tag{58}$$

In the above discussion, the initial guess $S_0(\eta)$, defined by Eq. (50), satisfies the boundary conditions (44). Hence, as we track the evolution of q across the range $[0,1]$, the solution of the zeroth-order deformation equation will vary continuously from the initial approximation $S_0(\eta)$ to the target function $S(\eta)$ that will exactly satisfy Eq. (44). Expanding $\Phi(\eta;q)$ in the Maclaurin series form with respect to q, we have

$$\Phi(\eta;q)=S_0(\eta)+\sum_{m=1}^{+\infty} S_m(\eta)q^m, \tag{59}$$

where

$$S_m(\eta)=\frac{1}{m!}\left.\frac{\partial^m\Phi(\eta;q)}{\partial q^m}\right|_{q=0}. \tag{60}$$

Here, the relationship $\Phi(\eta;0)=S_0(\eta)$ is used. It should be emphasized that the zeroth-order deformation equation (41) contains the convergence-control parameter $\hbar$, which is used to guarantee the convergence of the final series solution. In principle, $\hbar$ is chosen so that the above series remains convergent at $q=1$ over the entire domain, $\eta\in[0,1]$. Then, using the relationship $\Phi(\eta;1)=S(\eta)$, we obtain the homotopy-series solution

$$S(\eta) = S_0(\eta) + \sum_{m=1}^{+\infty} S_m(\eta), \tag{61}$$

where $S_m(\eta)$ is unknown. Its governing equation and related boundary conditions have to be carefully established. To this end, we introduce the vector

$$\vec{S}_m = \{S_0(\eta), S_1(\eta), S_2(\eta), \ldots, S_m(\eta)\}. \tag{62}$$

Differentiating the zeroth-order deformation equation (55) and the boundary conditions (56) m times with respect to q, dividing by $m!$, and then setting $q=0$, we obtain the so-called mth-order deformation equation

$$\mathcal{L}[S_m(\eta) - \chi_m S_{m-1}(\eta)] = \hbar\, \delta_m[S_{m-1}(\eta)]. \tag{63}$$

Equation (63) is subject to

$$\eta = 0: \quad S_m = 0, \quad S_m' = 0, \quad S_m'' = 0; \quad \eta = 1: \quad S_m = 0, \tag{64}$$

where

$$\chi_m = \begin{cases} 0, & m \le 1 \\ 1, & m > 1, \end{cases} \tag{65}$$

and the right-hand-side function δ_m is given by

$$\delta_m[S_{m-1}(\eta)] = S_{m-1}''''' + \alpha(3S_{m-1}'' + \eta S_{m-1}''') + R\sum_{n=0}^{m-1} (S_n S_{m-1-n}''' + S_n' S_{m-1-n}''). \tag{66}$$

According to Eq. (51), it is straightforward to retrieve a particular solution $S_m^*(\eta)$ of Eq. (63) by integrating the right-hand-side term four times with respect to η, viz.

$$S_m^*(\eta) = \chi_m S_{m-1}(\eta) + \hbar \int\int\int\int \delta_m(\vec{S}_{m-1}, \eta) d\eta d\eta d\eta d\eta. \tag{67}$$

The ensuing quadfold integration yields

$$S_m(\eta) = S_m^*(\eta) + C_{m,0} + C_{m,1}\eta + C_{m,2}\eta^2 + C_{m,3}\eta^3 \quad (m \ge 1), \tag{68}$$

where the integral constants

$$C_{m,0} = C_{m,2} = 0, \quad C_{m,1} = -\left.\frac{dS_m^*}{d\eta}\right|_{\eta=0}, \quad \text{and} \quad C_{m,3} = -C_{m,1} - S_m^*(1) \tag{69}$$

are secured from the boundary conditions in Eq. (64). The Mth-order approximation of $S(\eta)$ may hence be written as

$$S(\eta) \approx S_0(\eta) + \sum_{k=1}^{M} S_k(\eta). \tag{70}$$

Note that the above expression incorporates the unknown parameter γ.

The next step is to determine the value of γ that will permit the solution to satisfy the boundary condition (45) at the upper end of the domain, namely, $S'(1)=0$. Substituting the Mth-order approximation (70) into Eq. (45) gives

$$\Gamma_M(\gamma,\hbar) = S_0'(1) + \sum_{n=1}^{M} S_n'(1) = 0, \tag{71}$$

where Γ_M represents the expanded form of the constrained boundary condition. Using an Mth-order approximation, we have

$$S_M(\eta) = \sum_{n=0}^{3M+2} A_{M,n}(\alpha,\gamma,\hbar)\,\eta^{2n+1} \tag{72}$$

and so

$$\Gamma_M(\gamma,\hbar) = \sum_{n=0}^{M+1} B_{M,n}(\alpha,\hbar)\,\gamma^n = 0, \tag{73}$$

where $A_{M,n}(\alpha,\gamma,\hbar)$ and $B_{M,n}(\alpha,\hbar)$ are coefficients of the power series of η. Note that, as long as $\hbar$ is given, the solutions of Eq. (71) may be readily obtained.

In our quest for an optimal value of $\hbar$, we use a technique that has been shown to produce a fast converging HAM approximation. In principle, the technique seeks to minimize the exact square residual error of Eq. (41) at the mth-order. This quantity is given by

$$\hat{E}_m(\gamma,\hbar) = \int_0^1 \left(\mathcal{N}\left[\sum_{n=0}^{m} S_n(\eta)\right]\right)^2 d\eta. \tag{74}$$

In practice, however, the evaluation of $\hat{E}_m(\gamma,\hbar)$ tends to be time-consuming. A simpler alternative consists of calculating the averaged square residual error. In this vein, one may seek to minimize the zeroth-order discretization of Eq. (74),

$$E_m(\gamma,\hbar) = \frac{1}{(M+1)}\sum_{k=0}^{M}\left(\mathcal{N}\left[\sum_{n=0}^{m} S_n(\eta_k)\right]\right)^2, \tag{75}$$

where

$$\eta_k = k\Delta\eta = \frac{k}{M}, \quad k = 0,1,2,3,\ldots,M. \tag{76}$$

Hereafter, a value of $M=40$ will be used with the purpose of optimization. For traditional problems in which E_m is only dependent on $\hbar$, it is relatively straightforward to seek an optimal value $\hbar^*$ for which E_m is minimized. However, for the problem under consideration, the residual error is exacerbated by its dependence on both $\hbar$ and γ. In fact, both $E_m(\gamma,\hbar)$ and $\Gamma_M(\gamma,\hbar)$ contain the two unknowns: γ and $\hbar$. So, while the optimal convergence-control parameter $\hbar^*$ can still be determined from the minimum of $E_m(\gamma,\hbar)$, it must be additionally subjected to the algebraic equation (71) needed to secure the boundary value constant γ. For this doubly coupled optimization problem, we let $(\hbar^*,\gamma^*)$ denote the solution of the algebraic equation (71), which corresponds to the minimum of the square residual error. Mathematically, it holds that

$$(\hbar^*, \gamma^*) = \min\{E_m(\gamma,\hbar), \Gamma_m(\gamma,\hbar) = 0\}. \tag{77}$$

For the sake of computational efficiency, the exact square residual error may be replaced by the averaged square residual error (75). To identify the optimal approximation in a region $a \le \gamma \le b$, we take

$$(\hbar^*, \gamma^*) = \min\{E_m(\gamma,\hbar), \Gamma_m(\gamma,\hbar) = 0, a \le \gamma \le b\}. \tag{78}$$

Such an operation may be relegated to symbolic programming with a dedicated "Minimize" command.

Before leaving this section, it may be helpful to remark that Eq. (63), the high-order deformation equation represents a linear ODE that is relatively simple to solve. This behavior is contrary to that of Eq. (41), the original nonlinear ODE for uniform wall expansion with α=const. Using homotopy, the Dauenhauer–Majdalani ODE is transferable into an infinite number of linear ODEs that can be solved directly. The ensuing transformations are made possible by the flexibility of the HAM procedure in identifying a simple auxiliary linear operator through which the solution of the high-order deformation equation can be readily obtained. Meanwhile, the so-called convergence-control parameter $\hbar$ may be optimized to the extent of accelerating or ensuring the convergence of the series approximations.[28–31,41] These particular characteristics represent some of the key features that distinguish HAM from other analytical methods.

C. Multiple solutions

For constant α, Dauenhauer and Majdalani[20] obtained an exact ODE and provided the steps that can lead to a numerical solution using a fast-converging shooting method coupled with Runge–Kutta integration. They illustrated their results by providing numerical solutions over a modest range of R and α that are aligned with the type I family of solutions classified by Zaturska *et al.*[11] However, solutions of types II and III for the suction case, particularly those leading to internal flow steepening and recirculation, were alluded to but not considered in their article. Later studies by Majdalani and Zhou,[21] Majdalani *et al.*,[22] and Zhou and Majdalani[23] provided closed-form explicit approximations over some limited ranges of suction and injection.

To illustrate how the general HAM approach may be applied, we first consider a special case of α=4 and R=−10. We can sequentially solve up to the mth-order deformation equations (63) and (64) for $m=1,2,3,\ldots$. We hence retrieve

$$\begin{aligned} S_1(\eta) = {} & \hbar\left(\frac{\gamma^2}{77} + \frac{3173\gamma}{6930} - \frac{325}{924}\right)\eta^3 - \hbar\left(\frac{3\gamma}{5} - \frac{1}{2}\right)\eta^5 \\ & + \hbar\left(\frac{2\gamma^2}{21} - \frac{\gamma}{7} + \frac{1}{28}\right)\eta^7 \\ & - \hbar\left(\frac{10\gamma^2}{63} - \frac{55\gamma}{126} + \frac{25}{84}\right)\eta^9 \\ & + \hbar\left(\frac{5\gamma^2}{99} - \frac{5\gamma}{33} + \frac{5}{44}\right)\eta^{11}, \end{aligned} \tag{79}$$

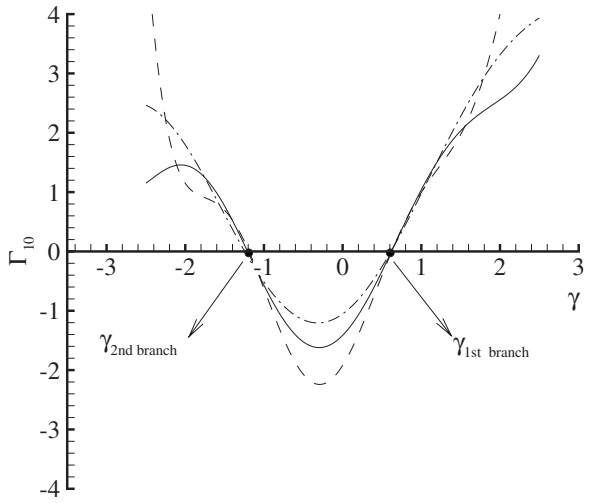

FIG. 4. Curves of $\Gamma_m(\gamma,\hbar)$ using a 10th-order HAM approximation (m=10) in case of R=−10 and α=4. Solid line: $\hbar$=−1; dashed line: $\hbar=-\frac{3}{2}$; dash-dotted line: $\hbar=-\frac{2}{3}$.

$$\begin{aligned} S_2(\eta) = S_1(\eta) + \hbar^2\Bigg(& \frac{63\,355\gamma^3}{6\,432\,426} - \frac{15\,323\,311\gamma^2}{192\,972\,780} \\ & + \frac{159\,557\,617\gamma}{643\,242\,600} - \frac{396\,889}{2\,450\,448}\Bigg)\eta^3 + \cdots. \end{aligned} \tag{80}$$

At the mth-order of approximation, $S_m(\eta)$ contains the unknown convergence-control parameter $\hbar$ and the unknown variable γ that satisfies the right-hand-side boundary condition connected with Eq. (71). At the first- and second-order approximations, Eq. (71) yields

$$\Gamma_1 = \hbar\left(\frac{41}{154} - \frac{421\gamma}{1155} - \frac{116\gamma^2}{693}\right) = 0 \tag{81}$$

and

$$\begin{aligned} \Gamma_2 = {} & \hbar\left(\frac{41}{77} - \frac{842\gamma}{1155} - \frac{232\gamma^2}{693}\right) + \hbar^2\Bigg(\frac{3215}{37\,128} \\ & - \frac{24\,693\,629\gamma}{107\,207\,100} + \frac{773\,027\gamma^2}{6\,432\,426} - \frac{2033\gamma^3}{153\,153}\Bigg) = 0, \end{aligned} \tag{82}$$

respectively, up to Γ_m. Thus, the algebraic equation $\Gamma_m(\gamma,\hbar)$=0 contains not only the unknown variable γ but also the unknown convergence-control parameter $\hbar$. Each zero γ^* of $\Gamma_m(\gamma^*,\hbar)$=0 will hence signal the presence of a distinct solution. After determining the number of zeros, a proper choice of $\hbar$ can be sought for each γ^*. It can thus be seen that the convergence-control parameter $\hbar$ has no physical meaning besides granting us the freedom to calibrate its value to the extent of optimizing the solution. For example, in case of the tenth-order approximation for R=−10 and α=4, the curves of $\Gamma_{10}(\gamma,\hbar)$ for $\hbar=-\frac{3}{2}, -1$ and $-\frac{2}{3}$ are computed and illustrated in Fig. 4. It is interesting that, although $\Gamma_{10}(\gamma,\hbar)$ curves are sensitive to the value taken by $\hbar$, the zeros of the algebraic equation $\Gamma_{10}(\gamma,\hbar)$=0 when $\hbar \in [-\frac{3}{2}, -\frac{2}{3}]$ remain close. They actually become virtually indiscernible as m is increased. The zeros appear to be only weakly sensitive to $\hbar$ despite the existence of two zeros in the re-

TABLE I. The optimal convergence-control parameter $\hbar^*$ and the corresponding averaged square residual error for the first $(\gamma>0)$ and second solutions $(\gamma<0)$ in the case of $R=-10$ and $\alpha=4$.

	m, order of approximation	$\hbar^*$	γ^*	$E_m(\gamma^*,\hbar^*)$
First solution	1	−0.886	0.577 336	32.33
	5	−1.022	0.609 118	5.25×10^{-2}
	10	−1.727	0.624 117	1.37×10^{-3}
	15	−1.764	0.624 840	8.07×10^{-5}
	20	−1.770	0.624 963	6.11×10^{-6}
Second solution	5	−1.303	−1.236 36	2.40
	10	−1.479	−1.190 69	0.11
	15	−1.515	−1.188 51	2.56×10^{-2}
	20	−1.458	−1.189 79	2.26×10^{-4}

TABLE III. The $[m,m]$ homotopy-Padé approximation of the first $(\gamma>0)$ and second solutions $(\gamma<0)$ in the case of $R=-10$ and $\alpha=4$.

	First solution		Second solution	
m	$F'(0)/R$	$F'''(0)/R$	$F'(0)/R$	$F'''(0)/R$
4	0.624 478 732	8.265 444 222	−1.219 891	36.010 91
8	0.625 005 336	8.255 477 422	−1.178 465	35.178 78
12	0.625 007 412	8.255 446 248	−1.190 349	35.854 62
16	0.625 007 395	8.255 446 127	−1.190 319	35.854 09
18	0.625 007 396	8.255 446 127	−1.190 319	35.854 11
20	0.625 007 396	8.255 446 125	−1.190 323	35.854 15
22	0.625 007 396	8.255 446 124	−1.190 323	35.854 16
24	0.625 007 396	8.255 446 124	−1.190 323	35.854 16

gions $\gamma\in(-2,-1)$ and $\gamma\in(0,1)$. Each of these zeros corresponds to a distinct solution.

At the given order of approximation m, the optimal convergence-control parameter $\hbar^*$ may be determined for the positive solution of $\gamma\in(0,1)$ by minimizing the averaged square residual error, specifically

$$(\hbar^*,\gamma^*)=\min\{E_m(\gamma,\hbar),\Gamma_m(\gamma,\hbar)=0,\gamma>0\}. \tag{83}$$

The first and second sets of outcomes obtained for $\hbar^*$ and γ^* through minimization are cataloged in Table I at different approximation orders. It is clear that as the order of approximation increases, the optimal convergence-control parameter $\hbar^*$ tends to -1.766 for the first solution, while the attendant γ^* approaches a positive value of approximately 0.625 00. It may be seen that $E_m(\gamma^*,\hbar^*)$, the averaged square residual error entailed in this analysis, decreases monotonically as m is increased. For the second solution, $\hbar^*$ tends to -1.5 while γ^* approaches a negative value of $-1.189\,79$. Here, too, the averaged square residual error $E_m(\gamma^*,\hbar^*)$ decreases monotonically as well.

For $R=-10$ and $\alpha=4$, the analytical approximations of $F_\eta(0)/R$ and $F'''(0)/R$ are listed in Table II for the two solutions at hand. While the set $F'(0)/R\approx0.625\,007$ and $F'''(0)/R\approx8.255\,45$ corresponds to the first solution, a second set is obtained for the second solution with $F'(0)/R\approx-1.190\,33$ and $F'''(0)/R\approx35.8542$. As the order of approximation is increased, the averaged square residual error is seen to decrease monotonically down to 7.99×10^{-8}; in the meantime, $F'(0)/R$ and $F'''(0)/R$ asymptotically converge to fixed values.

As shown in Fig. 4, there also exists a negative solution for $\gamma\in(-2,-1)$. At the prescribed order of approximation m, the companion parameter $\hbar^*$ may be determined from

$$(\hbar^*,\gamma^*)=\min\{E_m(\gamma,\hbar),\Gamma_m(\gamma,\hbar)=0,\gamma<0\}. \tag{84}$$

The convergence ratio of the homotopy-series solution can be accelerated by means of the so-called homotopy-Padé technique.[27–31] As shown in Table III, the homotopy-Padé technique enables us to identify the convergent approximation $F'(0)/R\approx0.625\,007\,396$ and $-1.190\,323$ for the first and second solutions, respectively. These predictions agree quite well with the numerical values of 0.625 007 4 and $-1.190\,323$ reported for these cases. Note that our analytical projections agree well with those reproduced using Dauenhauer and Majdalani's numerical approach.[20] These are shown in Fig. 5 where the axial flow velocity is illustrated using the numerical solution alongside a 20th-order HAM approximation. The two featured solutions are acquired using $\hbar=-\frac{7}{4},\frac{3}{2}$ at a crossflow Reynolds number of $R=-10$ and a wall expansion ratio of $\alpha=4$. In short, this example illustrates how the homotopy-based approach can

TABLE II. The mth-order approximation of the first $(\gamma>0)$ and second solutions $(\gamma<0)$ in the case of $R=-10$ and $\alpha=4$.

	$\hbar$	m, order of approximation	$F'(0)/R$	$F'''(0)/R$	$E_m(\gamma,\hbar)$
First solution	$-\frac{7}{4}$	10	0.624 161	8.267 56	1.51×10^{-3}
		20	0.624 967	8.256 03	6.55×10^{-6}
		30	0.625 005	8.255 48	3.68×10^{-8}
		40	0.625 007	8.255 45	1.81×10^{-10}
		50	0.625 007	8.255 45	1.11×10^{-12}
Second solution	$-\frac{3}{2}$	10	−1.189 95	35.8984	0.150
		20	−1.190 03	35.8474	6.54×10^{-4}
		30	−1.190 41	35.8555	1.05×10^{-5}
		40	−1.190 31	35.8539	8.46×10^{-7}
		50	−1.190 33	35.8542	7.99×10^{-8}

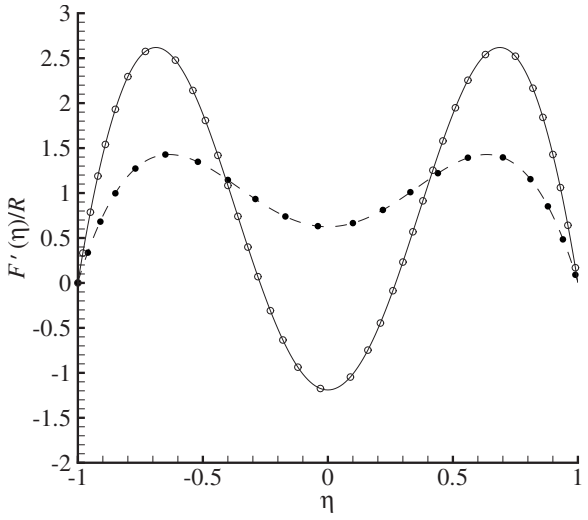

FIG. 5. Comparison of numerical solutions with the 20th-order HAM approximation for $F'(\eta)/R$ in case of $R=-10$ and $\alpha=4$. Symbols: numerical results; dashed line: first solution with $\hbar=-\frac{7}{4}$; solid line: second solution with $\hbar=-\frac{3}{2}$.

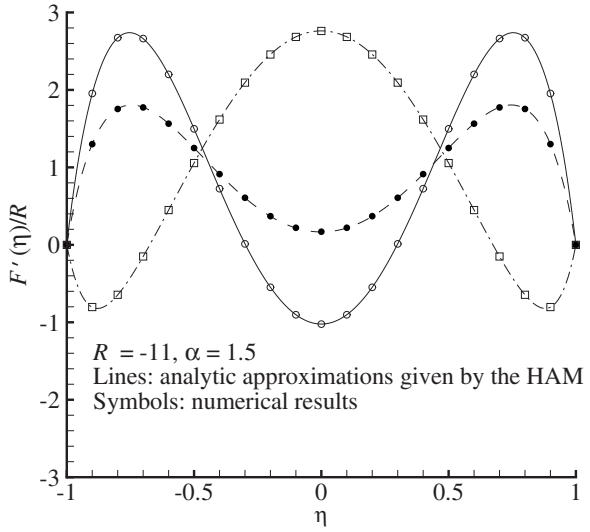

FIG. 7. Comparison of numerical solutions with the 30th-order HAM approximation of $F'(\eta)/R$ in case of $R=-11$ and $\alpha=\frac{3}{2}$. Symbols: numerical results; solid line: first solution with $\hbar=-\frac{5}{3}$; dashed line: second solution with $\hbar=-\frac{5}{3}$; dash-dotted line: third solution with $\hbar=-\frac{3}{4}$.

indeed capture the dual solutions of the nonlinear boundary-value problem for channel flows with constant wall expansion.

The present approach is capable of capturing triple roots when three branches of solution arise. A concrete example consists of the case of $R=-11$ and $\alpha=1.5$. The corresponding curves of $\Gamma_{10}(\gamma,\hbar)$ at the tenth order of approximation are given in Fig. 6 using $\hbar=-1$, $-\frac{3}{2}$, and $-\frac{2}{3}$. This graph clearly shows that two values of γ emerge near -1 and 0. Besides, it appears that a third solution exists in the region of $\gamma>1$. In the case of $R=-11$ and $\alpha=1.5$, Eq. (71) produces three solutions near -1, 0, and $\gamma>1$. In seeking an optimal convergence-control parameter, we carefully bracket our searches within the following intervals:

$$\text{(A):}\quad \min\{E_m(\gamma,\hbar),\quad \Gamma_m(\gamma,\hbar)=0,\quad -2<\gamma\leq -0.5\}, \tag{85}$$

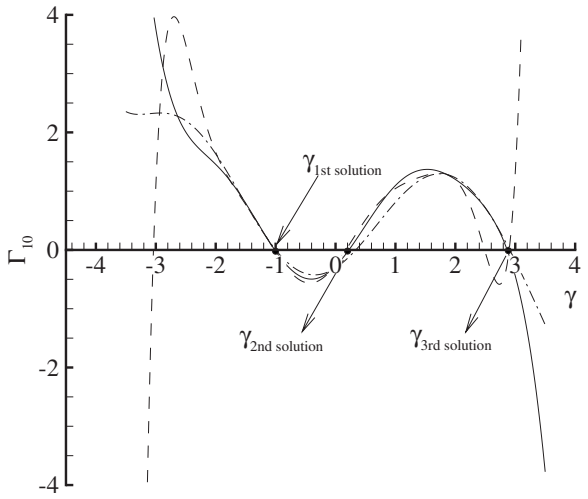

FIG. 6. Curves of $\Gamma_m(\gamma,\hbar)$ using a tenth-order HAM approximation ($m=10$) in case of $R=-11$ and $\alpha=1.5$. Solid line: $\hbar=-1$; dashed line: $\hbar=-\frac{3}{2}$; dash-dotted line: $\hbar=-\frac{2}{3}$.

$$\text{(B):}\quad \min\{E_m(\gamma,\hbar),\quad \Gamma_m(\gamma,\hbar)=0,\quad -0.5<\gamma\leq 0.5\}, \tag{86}$$

$$\text{(C):}\quad \min\{E_m(\gamma,\hbar),\quad \Gamma_m(\gamma,\hbar)=0,\quad 0.5<\gamma\leq 4\}. \tag{87}$$

Forthwith, the results of our analysis are posted in Table IV. We find $\hbar^*$ to be approximately $-\frac{5}{3}$ for the first and second solutions, and $-\frac{4}{5}$ for the third. The HAM approximations of $F'(0)/R$ and $F'''(0)/R$ associated with these three solutions are listed in Table V. Using the homotopy-Padé technique, we obtain $F'(0)/R=-1.023\,771\,2$ and $0.169\,352$ for the first and second solutions, respectively. These values agree very well with the numerical predictions of $F'(0)/R=-1.023\,771$ and $0.169\,353\,2$ for these two branches. In contrast, we find the third solution to be more difficult to retrieve. This may be attributed to its averaged square residual error remaining 5.68×10^{3} at the tenth-order approximation and slowly decreasing to 1.08×10^{-3} at the 60th order (see Table VI). Everywhere, the three analytical approximations of $F'(\eta)/R$ appear to be in excellent agreement with the numerical predictions shown in Fig. 7. This uniformly consistent agreement with numerics is realized owing, in large part, to the ability of the HAM approximation to capture the true, nonlinear behavior of the solution in the limit of an infinite series.

Generally speaking, the numerical identification of all possible solutions associated with nonlinear boundary-value problems can require significant effort. For the suction driven channel flow with no wall motion, Zaturska *et al.*[11] showed that one symmetric solution exists for $R\in[-12.165,0]$ and three symmetric solutions emerge when $R\in[-\infty,-12.165]$. In the present work, the same types of solutions are captured. Using HAM, dual solutions are returned, for example, in the case of $R=-10$ and $\alpha=4$, while three distinct solutions are retrieved in the case of $R=-11$ and $\alpha=1.5$. The accuracy of our analytical predictions may

TABLE IV. The optimal convergence-control parameter $\hbar^*$ and the corresponding averaged square residual error in the case of $R=-11$ and $\alpha=1.5$ for three solutions of γ^*.

	m, order of approximation	$\hbar^*$	γ^*	$E_m(\gamma^*,\hbar^*)$
First solution	4	−1.235	−0.982 73	11.9
	8	−1.604	−1.020 08	0.153
	12	−1.561	−1.022 75	2.37×10^{-2}
	16	−1.654	−1.023 56	2.49×10^{-4}
	20	−1.625	−1.023 71	1.16×10^{-4}
Second solution	6	−1.661	0.212 76	24.6
	8	−1.701	0.176 35	2.18
	12	−1.441	0.166 88	2.40×10^{-2}
	16	−1.146	0.167 17	1.69×10^{-2}
	20	−1.681	0.169 45	5.95×10^{-4}
Third solution	20	−0.951	2.753 98	17.3
	24	−0.859	2.757 36	12.2
	26	−0.940	2.750 98	2.70
	28	−0.881	2.759 36	1.09
	30	−0.875	2.766 89	0.37

TABLE V. The mth-order approximation of the three solutions in the case of $R=-11$ and $\alpha=\frac{3}{2}$.

	$\hbar$	m, order of approximation	$F'(0)/R$	$F'''(0)/R$	$E_m(\gamma,\hbar)$
First solution	$-\frac{5}{3}$	10	−1.022 322	24.270 70	0.468
		20	−1.023 716	24.285 64	1.52×10^{-4}
		30	−1.023 769	24.286 28	1.60×10^{-7}
		40	−1.023 771	24.286 31	5.01×10^{-10}
		50	−1.023 771	24.286 31	1.72×10^{-12}
Second solution	$-\frac{5}{3}$	10	0.166 208	10.2842	0.67
		20	0.169 384	10.2447	7.20×10^{-4}
		30	0.169 378	10.2449	2.19×10^{-5}
		40	0.169 335	10.2452	9.98×10^{-7}
		50	0.169 354	10.2451	3.49×10^{-8}
Third solution	$-\frac{3}{4}$	20	2.779 59	−15.6613	$3.62\times10^{+2}$
		30	2.762 18	−15.5188	$1.49\times10^{+1}$
		40	2.761 14	−15.5128	0.30
		50	2.761 24	−15.5134	7.40×10^{-3}
		60	2.761 11	−15.5122	1.08×10^{-3}

TABLE VI. The $[m,m]$ homotopy-Padé approximation of three solutions in the case of $R=-11$ and $\alpha=\frac{3}{2}$.

	First solution		Second solution		Third solution	
m	$F'(0)/R$	$F'''(0)/R$	$F'(0)/R$	$F'''(0)/R$	$F'(0)/R$	$F'''(0)/R$
4	−1.023 162 1	24.292 585 1	0.166 859 0	10.282 860	⋯	⋯
8	−1.023 770 0	24.286 379 7	0.167 998 0	10.239 451	2.815 91	−15.8950
12	−1.023 771 1	24.286 308 6	0.169 360 1	10.245 072	2.762 90	−15.5284
16	−1.023 771 2	24.286 308 8	0.169 351 8	10.245 026	2.761 54	−15.5157
20	−1.023 771 2	24.286 308 8	0.169 353 2	10.245 150	2.761 13	−15.5123
22	−1.023 771 2	24.286 308 8	0.169 353 1	10.245 152	2.761 11	−15.5123
24	−1.023 771 2	24.286 308 8	0.169 353 2	10.245 151	2.761 11	−15.5123

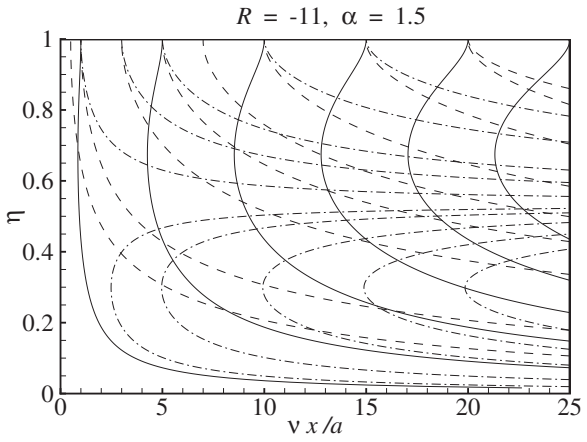

FIG. 8. Streamline patterns of three types of analytical solutions in case of $R=-11$ and $\alpha=\frac{3}{2}$. Solid line: type I solution with $F'(0)/R=2.761\ 11$; dashed line: type II solution with $F'(0)/R=0.169\ 353\ 2$; dash-dotted line: type III solution with $F'(0)/R=-1.023\ 771\ 190$.

hence be viewed as supportive of the potential application of HAM as a guide, if not alternative, to numerical solutions of nonlinear boundary-value problems, particularly, of those arising in fluid mechanics.

It is clear that our solutions correspond to the three types of mean flow profiles discussed by Zaturska *et al.*[11] in the case of a stationary porous wall. Due to the striking similarities between our analytical solutions and theirs, we have labeled our branches after theirs. This behavior is expected because the problem related to the porous channel flow with stationary walls should be recoverable from our analysis in the limiting case of $\alpha=0$.

To showcase the flow behavior corresponding to the different branches of solution, fluid streamlines are plotted in Fig. 8 for $\alpha=1.5$ and $R=-11$. This graph depicts all three types of solutions and enables us to deduce their fundamental characteristics under conditions conducive of wall suction.

Overall, both types I and II share a similar characteristic; it is possible for the flow drawn at the porous wall to originate from the chamber volume bounded anywhere between $0\leq r\leq 1$. By way of contrast, it may be seen that the type II profile undergoes faster flow turning above the porous wall, as corroborated by the sharper streamline curvatures depicted in Fig. 8. For the type III profile, the fluid removed at the surface may only originate from an annular region that extends over $\Delta\leq r\leq 1$. In the case of a nonexpanding wall ($\alpha=0$), an expression for the inner distance Δ of the type III annulus may be determined using a transcendental relation that can be obtained asymptotically for $R\rightarrow-\infty$. As shown by Lu,[42] this relation is given by

$$(R\Delta)\exp(-R\Delta)=-\frac{R^8}{2\pi^9\exp(1)}, \tag{88}$$

where R is negative for wall suction. Lu's type III solution emerges asymptotically and may be described by the compact trigonometric function,

$$F(y)=-\frac{1-\Delta}{\pi\Delta}\sin\left(\frac{\pi y}{1-\Delta}\right). \tag{89}$$

At this juncture, it may be useful to remark that the curvature disparity between the first two types will gradually vanish with increasing $|R|$. This is due to the convergence of the two branches onto a single polynomial expression that is elaborately discussed by Robinson[7] and Zaturska *et al.*[11] Accordingly, the type I and type II branches collapse into the essentially irrotational form,

$$F(y)=y+O(R^{-1});\quad R\rightarrow-\infty. \tag{90}$$

Along similar lines, only one solution is confirmed for small suction with $R\in[-12.165,0]$. This is given by

$$F(y)=\tfrac{1}{2}y(3-y^2);\quad R\rightarrow 0^-. \tag{91}$$

When attention is turned to injection dominated conditions, the unique branch for the small suction case continues to hold as the crossflow Reynolds number undergoes a sign switch. Two asymptotic solutions are known to date and these correspond to either small or large injection Reynolds numbers. According to Berman,[1] the small injection mean flow solution remains identical to the one obtained for small suction, namely,

$$F(y)=\tfrac{1}{2}y(3-y^2);\quad R\rightarrow 0^+. \tag{92}$$

However, as the crossflow Reynolds number is increased, a trigonometric solution emerges, specifically

$$F(y)=\sin\left(\tfrac{1}{2}\pi\right);\quad R\rightarrow+\infty. \tag{93}$$

Equation (93) for the large injection case has often been termed "Taylor's profile" due to its relevance to several technological applications that encompass paper manufacture and both solid and hybrid propellant gas dynamics.

Before leaving this subject, it may be instructive to remark that, at first, we have initiated our analysis by exploring the type I HAM solutions for which $F(y)=\frac{1}{2}y(3-y^2)$ represents a valid initial approximation for the problem targeted by Dauenhauer and Majdalani.[20] We have then extended our analysis by uncovering the additional types II and III without changing the initial guess function. We have thus significantly broadened the range of applicability of analytical representations for the types II and III branches beyond those achieved asymptotically in previous studies. These include several asymptotic solutions developed by Majdalani and co-workers[21–23] over some special ranges of R and $\alpha\neq 0$. It must be borne in mind, however, that the types II and III branches of solutions are expected to be mostly unstable according to the projections made by Zaturska *et al.*,[11] Lu *et al.*,[25] and MacGillivray and Lu.[24]

As we explore wider ranges of α and R using our HAM-based approach, we find that when $-10.727\ 376\leq R\leq-8.704\ 297\ 0$, dual solutions are possible for some values of α. In this situation, when the values of $F'(0)$ are plotted versus α in a range of R, a closed circle is formed, as shown in Fig. 9. Our analytical solutions agree with the numerical results given by the shooting integration method. Specifically, the value of $F'(0)$ shown on the graph corresponds to

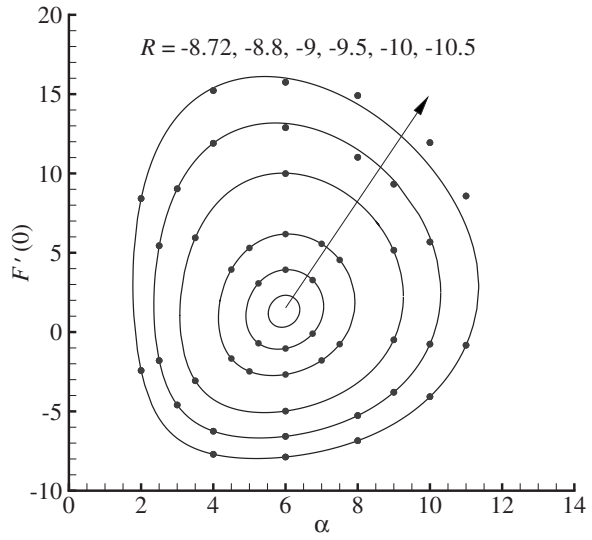

FIG. 9. Multiple solutions for varying R and α (suction conditions). Symbols: analytical results given by the HAM-based approach; line: numerical results given by the shooting method.

the axial velocity evaluated along the channel's midsection plane. The presence of dual or triple solutions will thus lead to dissimilar mean flow profiles.

IV. SOLUTIONS FOR TIME-DEPENDENT WALL EXPANSION RATIOS

The analysis so far has been centered on the assumption that α remains constant during the expanding or contracting motions of the porous wall. In what follows, we relax this condition and allow the wall expansion ratio to become time variant. This enables us to test the validity of the original assumption leading to the exact Navier–Stokes reduction. Our choice of $\alpha(t)$ is guided by the formulations presented through Eqs. (18)–(21). For example, by taking

$$\alpha(t) = \alpha_0 \exp(-t) + \alpha_1[1 - \exp(-t)], \tag{94}$$

we obtain

$$\beta(t) = -2\alpha_0 \exp(-t) + 2\alpha_1 t + 2\alpha_1 \exp(-t). \tag{95}$$

It can thus be seen that the wall expansion ratio $\alpha(t)$ varies exponentially. If we further assume that α_0 and α_1 represent the initial and final values of $\alpha(t)$, we can put

$$\alpha(t) = \alpha_1 + (\alpha_1 - \alpha_0)\frac{t}{1+t}, \tag{96}$$

whence

$$\beta(t) = 2\alpha_1 t + 2(\alpha_0 - \alpha_1)\log(1+t). \tag{97}$$

In what follows, we find it useful to employ the algebraic approximations (96) and (97) in lieu of the exponentially decaying forms given by Eqs. (94) and (95). In the present case, we solve a nonlinear PDE, here Eq. (21), with the boundary conditions given by Eq. (17). In general, a nonlinear PDE is substantially more challenging to solve than an ODE, even by means of numerical techniques. Besides, PDEs are traditionally regarded as fundamentally different from ODEs. So the question that comes to mind is this: Can we transform a nonlinear PDE into an infinite number of linear ODEs? The answer is positive: in many cases,[30] a nonlinear PDE can be indeed broken down into a sequence of linear ODEs by means of homotopy.[41] The analytical treatment of a nonlinear, unsteady PDE with a time-dependent wall expansion ratio $\alpha(t)$ is rather similar to that employed in the treatment of a nonlinear ODE with constant α. The procedure is straightforward and so, in the interest of brevity, the steps are outlined below and further detailed in the Appendix. First, $F(\eta,t)$ is expressed by a series

$$F(\eta,t) = F_0(\eta,t) + \sum_{m=1}^{+\infty} F_m(\eta,t), \tag{98}$$

where $F_m(\eta,t)$ is controlled by the high-order deformation equation

$$\mathcal{L}[F_m(\eta,t) - \chi_m F_{m-1}(\eta,t)] = \hbar\,\hat{\delta}_m(\eta,t) \tag{99}$$

with

$$F_m(0,t) = 0,$$
$$\left.\frac{\partial^2 F_m}{\partial \eta^2}\right|_{\eta=0} = 0, \quad F_m(1,t) = 0, \quad \left.\frac{\partial F_m}{\partial \eta}\right|_{\eta=1} = 0, \tag{100}$$

in which

$$\hat{\delta}_m(\eta,t) = F'''_{m-1} + \alpha(t)(3F''_{m-1} + \eta F'''_{m-1}) - \beta(t)\dot{S}''_{m-1} + \sum_{n=0}^{m-1}(F_n F'''_{m-1-n} + F'_n F''_{m-i-n}). \tag{101}$$

Here, the primes and dots denote differentiation with respect to η and t, respectively, the auxiliary linear operator $\mathcal{L}$ is given by Eq. (A5), and χ_m is defined by Eq. (65). For simplicity, we choose a simple initial guess

$$F_0(\eta,t) = \tfrac{1}{2}R\eta(3 - \eta^2), \tag{102}$$

which satisfies Eq. (17). Subsequently, the nonlinear PDE defined by Eq. (21) may be converted into an infinite number of linear ODEs using HAM, as shown in the Appendix.

The sensitivity of the solution with respect to the choice of a time-dependent model for $\alpha(t)$ is illustrated in Fig. 10. Therein, the axial velocity profile is plotted at $R=1$ and several instants of time that correspond to a variation in $\alpha(t)$ from -2 to -1. It is interesting to note the general agreement between the two families of curves. As one may expect, the profiles using the exponentially decaying behavior for $\alpha(t)$ vary slightly more rapidly than those based on the algebraic approximation. Another case is illustrated in Fig. 11 where the axial velocity profile $F_\eta(0,t)$ is plotted as a function of t while $\alpha(t)$ is varied "to and fro" between 1 and 2. It is clear that the velocity decays monotonically when $\alpha(t)$ is reduced from 2 to 1; the converse is true as $\alpha(t)$ is incremented from 1 to 2. The significant outcome to report here is that, regardless of direction taken, the velocity profiles quickly approach the steady state conditions. Similar trends are displayed by other flow variables. This rapid shift to steady state behavior helps to confirm the validity of the analysis performed heretofore, specifically in Sec. III where

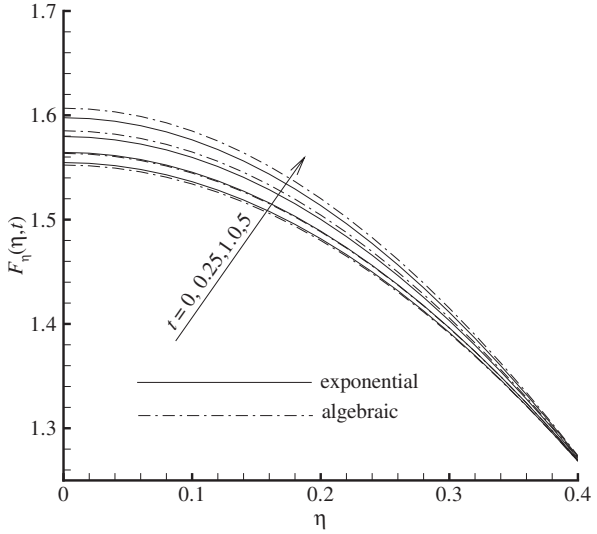

FIG. 10. Sensitivity of the axial velocity $F_\eta(\eta,t)$ at $R=1$ as $\alpha(t)$ is varied from $\alpha_0=-2$ to $\alpha_1=-1$.

the time dependence is deliberately ignored as a requirement to reduce the Navier–Stokes equations into a single, fourth order ODE.

To illustrate the time-dependent evolution of the axial velocity, Figs. 12(a) and 12(b) are used to depict the behavior of F' at two different injection coefficients, specifically, for $A=\pm 5$. These results correspond to the direct temporal solution of Eq. (21). To verify the rapid shift to steady state conditions, the axial velocity profiles are shown for $t=0,0.5,1.0,2.0,5.0,10.0$. Note that, at the scale used in these graphs, the curves beyond $t=5$ cannot be visually distinguished. Along similar lines, the spatial variation in the normal velocity is illustrated in Figs. 13 and 14. In Fig. 13, the sensitivity of the normal velocity is illustrated at three different wall expansion ratios, $\alpha=-5,0,+5$, hence including those caused by suction, stationary motion, or injection. These are computed using a 40th-order HAM approximation and a fixed crossflow Reynolds number of $R=5$. As for Fig. 14, it illustrates the time evolution of the normal velocity for $t=0,0.5,1.0,2.0,5.0$, an injection coefficient of $A=5$, and a time-dependent wall expansion ration that varies from -1 to -2. Here, too, results beyond $t=5.0$ become indiscernible, thus signaling the onset of steady state conditions.

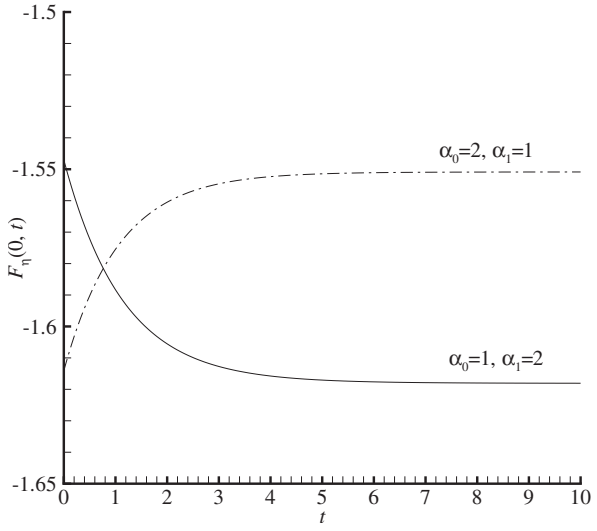

FIG. 11. Temporal variation in the centerline velocity $F_\eta(0,t)$ for $R=1$.

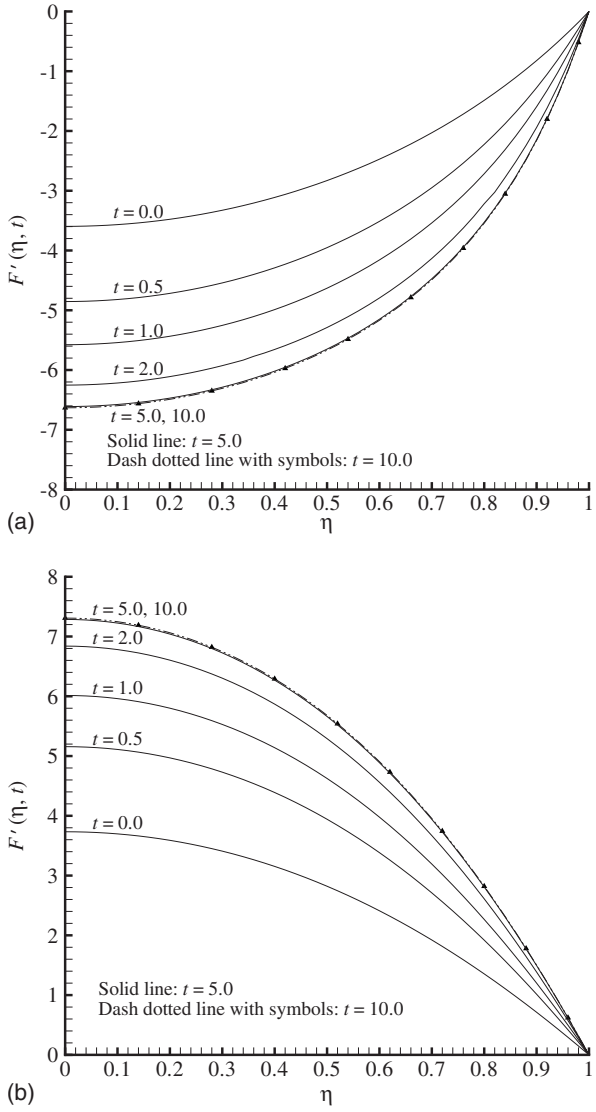

FIG. 12. Spatial variation in the axial velocity $F_\eta(\eta,t)$ for some values of t using (a) $A=-5$ and (b) $A=5$.

V. CONCLUSIONS

In this study, the porous channel with orthogonally moving walls is revisited in the context of laminar incompressible motion with both uniform and nonuniform wall regressions. The flow in the case of uniform wall regression is described by a nonlinear ODE, but the flow in the case of nonuniform wall regression is prescribed by a nonlinear PDE. For each case, an analytic approach based on the HAM is presented, thus transforming the original nonlinear ODE or PDE into an infinite number of linear ODEs whose solutions can be obtained by symbolic computation software. At the outset, a recursive series formulation is derived that can be readily evaluated using generic programming. The HAM-based procedure may thus be viewed as a technique that can

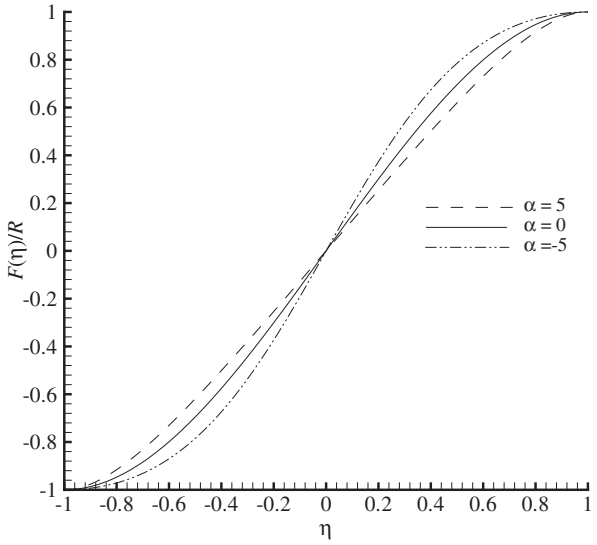

FIG. 13. Spatial variation in the normal velocity profile $F(\eta)/R$ using a 40th-order HAM approximation and three fixed values of α and $R=5$.

greatly simplify the solution of nonlinear ODEs or PDEs. In this endeavor, multiple solutions may be connected to a finite number of distinct zeros, here called γ^*, of a constraint equation associated with the shooting approach. After identifying the distinct solutions associated with each zero, a convergence-control parameter $\hbar$ may be carefully selected to ensure the convergence of the series at hand. In the present work, an error minimization approach is employed to determine an optimal value $\hbar^*$ that leads to fast series convergence. When necessary, the homotopy-Padé technique is invoked to further accelerate series convergence. At length, a series approximation is obtained for the nonlinear Dauenhauer–Majdalani ODE, in the case of constant wall expansion, and for the time-dependent PDE, in the case of a time-varying wall expansion.

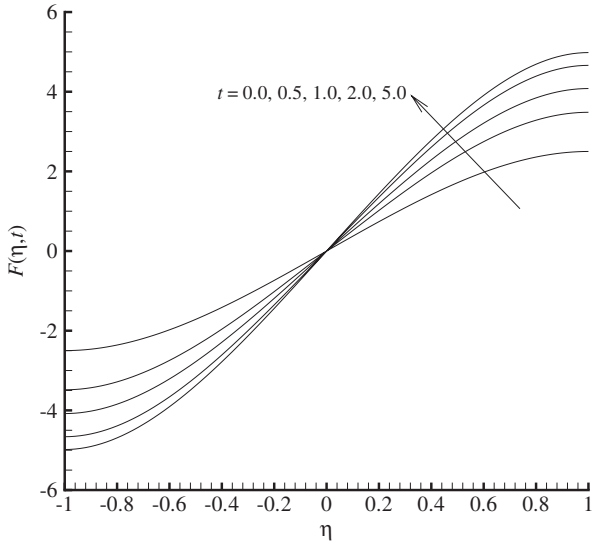

FIG. 14. Spatial variation in the normal velocity $F(\eta,t)$ using a [30,30] order homotopy-Padé approximation for some values of t and $A=5$. Here, $\alpha(t)$ evolves exponentially from -1 to -2.

For the uniform wall expansion ratio, our HAM-based approach is shown to capture dual and triple solutions in different ranges of R and α. We not only recover the type I branch of solutions pursued by Dauenhauer and Majdalani,[20] but also capture the type II and type III families reported by Zaturska *et al.*[11] These solutions were alluded to although not pursued in Dauenhauer and Majdalani's former article.[20] The new profiles involve either steeper flow turning at the wall (type II) or annular flow splitting and recirculation that are thoroughly described by Lu (type III). The high-order approximations presented here to describe all three categories of motion are shown to exhibit substantial agreement with the numerical results acquired using the integration algorithm constructed by Dauenhauer and Majdalani.[20]

For the nonuniform wall expansion case, two models for $\alpha(t)$ are chosen that involve either exponential or algebraic variation from an initial α_0 to a final α_1. With this assumption in effect, the Navier–Stokes equations are transformed into a PDE using a judicious choice of similarity variables. The resulting problem is solved analytically by HAM and shown to quickly reproduce the steady state solution obtained previously. This is due to the rapid decay of the time-dependent transients and the swift convergence of the solution to conditions corresponding to a constant wall expansion ratio.

Finally, it is clear that HAM offers several advantages when compared with other methods of solution. First, while the reduced ODE has been previously solved using asymptotics, its accuracy has remained dependent on the size of the small perturbation parameter $1/R$. Unlike the perturbation approximation that applies to a limited range of Reynolds numbers, the HAM solution has no limitations. It is not only independent of the size of $1/R$ but it also provides, as a windfall, a convenient tool that can be calibrated to ensure series convergence. Second, the process of identifying multiple solutions using HAM is facilitated, even in the case for which the multiplicity in the numerical solution becomes elusive. Third, the solution of the nonlinear PDE is made possible through the use of HAM, which could deal with both nonlinear ODEs and nonlinear PDEs with equal level of ease. The main benefits of HAM stand, perhaps, in its ability to solve a nonlinear equation using a parameter-free procedure that is so versatile that it can handle equally efficiently either a PDE or an ODE. Using similar tactics, our analytical approach can be further applied and incrementally modified to help in the identification of multiple steady and time-dependent solutions of a variety of nonlinear equations that arise in fluid mechanics, especially in the field of global flow stability.

ACKNOWLEDGMENTS

H.X., Z.-L.L., and S.-J.L. extend their sincere appreciation to the National Natural Science Foundation of China for the support through Grant Nos. 10972036, 50739004, and 10872129. S.-J.L. thanks the State Key Laboratory of Ocean Engineering for the partial support through Grant No. GKZD010002. J.-Z.W. is thankful for the partial support received from the Sate Key Laboratory for Turbulence and

Complex Systems, Peking University, China. Finally, J.M. is deeply grateful for the support received from the National Science Foundation, Grant No. CMMI-0928762, and through the travel supplement derived from the International Research and Education in Engineering (IREE) program on Grant No. CMMI-0353518.

APPENDIX: GENERAL PROCEDURE FOR SOLVING THE UNSTEADY EXPANSION RATIO PROBLEM

In what follows, we describe the mathematical steps needed to apply HAM to the porous channel flow problem with a time-dependent expansion ratio $\alpha(t)$. We thus consider the unsteady PDE given by Eq. (21). The attendant analysis encompasses the solution to Eq. (16), which can be recovered for $\alpha(t)=\frac{1}{2}$, $\dot{\beta}(t)=$const. The description to follow can thus be applied to both steady and unsteady cases.

To begin, the form of the analytical solutions to Eq. (21) must be posited in term of suitable functions. Depending on the character of $\beta(t)$ or $\alpha(t)$, different solution expressions are required. For the type I family of solutions that we seek here, three cases arise depending on the behavior of $\alpha(t)$. For $\alpha(t)=$const, F becomes independent of time; nonetheless, to present the procedure systematically for the three cases at hand, we still include t as we put

$$F(\eta,t)=\sum_{i=0}^{+\infty} B_i \eta^i. \tag{A1}$$

Next, we consider the unsteady $\alpha(t)=\alpha_0\exp(-t)+\alpha_1[1-\exp(-t)]$; the solution expression for the exponentially decaying behavior may be readily expressed as

$$F(\eta,t)=\sum_{i=0}^{\infty}\sum_{j=0}^{\infty}\sum_{k=0}^{\infty} B_{i,j}^{k}\eta^i t^j \exp(-kt). \tag{A2}$$

Finally, for $\alpha(t)=\alpha_1+(\alpha_1-\alpha_0)t/(1+t)$, the series representation for the algebraically varying expansion ratio may be written as

$$F(\eta,t)=\sum_{i=0}^{\infty}\sum_{j=0}^{\infty}\sum_{k=0}^{\infty}\sum_{s=0}^{\infty} B_{i,j}^{k,s}\eta^i t^j \frac{1}{(1+x)^k}[\ln(1+t)]^s. \tag{A3}$$

Here B_i, $B_{i,j}^{k}$, and $B_{i,j}^{k,s}$ are undetermined coefficients that we must seek to determine.

According to the homotopy-based approach, one needs to introduce an initial guess function of the form prescribed by the solution expressions while satisfying the problem's boundary conditions. For all three cases, a suitable choice corresponds to the leading order asymptotic solution obtained by Berman[1] at small Reynolds numbers, specifically

$$\phi_0(\eta,t)=\tfrac{1}{2}R\eta(3-\eta^2). \tag{A4}$$

Note that the above equation satisfies Eq. (11) and may be shown to be a viable candidate for the initial approximation of $F(\eta,t)$. An auxiliary linear operator $\mathcal{L}$ is then defined to the extent of capturing the highest order in Eq. (21). This is

$$\mathcal{L}[\Phi(\eta,t)]=\frac{\partial^4\Phi(\eta,t)}{\partial\eta^4}, \tag{A5}$$

which has the property

$$\mathcal{L}(C_0+C_1\eta+C_2\eta^2+C_3\eta^3)=0, \tag{A6}$$

where (C_0,C_1,C_2,C_3) are integral constants. This representation satisfies the rule of solution expression through which the linear approximation is constructed from the set of base functions. At this point, a homotopy mapping relation may be implemented of the type

$$\begin{aligned} &F:\eta,t\times[0,1]\mapsto H|\Phi(\eta,t;0)=\phi(\eta,t);\\ &\Phi(\eta,t;1)=F(\eta,t). \end{aligned} \tag{A7}$$

This transformation leads to the HAM deformation equation that has been well established as

$$(1-q)\mathcal{L}[\Phi(\eta,t;q)-\phi_0(\eta,t)]=q\hbar\mathcal{N}[\Phi(\eta,t;q)], \tag{A8}$$

where $q\in[0,1]$ is an embedding parameter and $\hbar$ is a nonzero auxiliary parameter known as the convergence-control parameter.[27] Note that $\mathcal{N}$ is a nonlinear operator obtained by recasting Eq. (21) into $\mathcal{N}[\Phi(\eta;q)]=0$. We, therefore, have

$$\begin{aligned} \mathcal{N}[\Phi(\eta;q)]=&\frac{\partial^4\Phi(\eta;q)}{\partial\eta^4}+\Phi(\eta;q)\frac{\partial^3\Phi(\eta;q)}{\partial\eta^3}\\ &+\frac{3}{2}\beta_i(t)\frac{\partial^2\Phi(\eta;q)}{\partial\eta^2}-\frac{\partial\Phi(\eta;q)}{\partial\eta}\frac{\partial^2\Phi(\eta;q)}{\partial\eta^2}\\ &+\frac{1}{2}\beta_i(t)\eta\frac{\partial^3\Phi(\eta;q)}{\partial\eta^3}-\beta(t)\frac{\partial^3\Phi(\eta;q)}{\partial\eta^2\,\partial t}. \end{aligned} \tag{A9}$$

The corresponding assortment of boundary conditions translates into

$$\begin{aligned} &\Phi(0,t;q)=0, \quad \left.\frac{\partial^2\Phi(\eta,t;q)}{\partial\eta^2}\right|_{\eta=0}=0,\\ &\Phi(1,t;q)=R, \quad \left.\frac{\partial\Phi(\eta,t;q)}{\partial\eta}\right|_{\eta=1}=0. \end{aligned} \tag{A10}$$

At this point, it may be instructive to note that when

$$\begin{cases} q=0: & \mathcal{L}[\Phi(\eta,t;0)-\phi_0(\eta,t)]=0,\\ q=1: & \mathcal{N}[\Phi(\eta,t;1)]=0; \quad \forall\,\hbar\neq 0. \end{cases} \tag{A11}$$

Hence as we track the evolution of q across the range $[0,1]$, the solution of the nonlinear equation will transition from the initial approximation $\phi_0(\eta)$ to the target function that will exactly satisfy Eq. (21). Expanding $\Phi(\eta,t;q)$ in the Maclaurin series form with respect to q, we have

$$\Phi(\eta,t;q)=\Phi_0(\eta,t,0)+\sum_{m=1}^{+\infty}\phi_m(\eta,t)q^m, \tag{A12}$$

where

$$\phi_m(\eta,t) = \frac{1}{m!} \left. \frac{\partial^m \Phi(\eta,t;q)}{\partial q^m} \right|_{q=0}. \tag{A13}$$

For brevity, we introduce a vector

$$\vec{\phi}_m = \{\phi_0(\eta,t), \phi_1(\eta,t), \phi_2(\eta,t), \ldots, \phi_m(\eta,t)\}. \tag{A14}$$

The next step consists of differentiating the HAM deformation equation (A8) m times with respect to q, dividing by $m!$, and then setting $q=0$. This enables us to obtain the m*th*-order deformation equation

$$\mathcal{L}[\phi_m(\eta,t) - \chi_m \phi_{m-1}(\eta,t)] = \hbar R_m[\phi_{m-1}(\eta,t)], \tag{A15}$$

which is subject to the boundary conditions

$$\eta = 0: \quad \phi_m = 0, \quad \phi_m'' = 0; \quad \eta = 1: \quad \phi_m = 0, \quad \phi_m' = 0. \tag{A16}$$

In Eq. (A15), the right-hand-side function R_m is given by

$$\begin{aligned} R_m[\phi_{m-1}(\eta,t)] &= \frac{1}{(m-1)!} \left. \frac{\partial^{m-1} \mathcal{N}[\Phi(\eta,t;q)]}{\partial q^{m-1}} \right|_{q=0} \\ &= \phi_{m-1}''' + \sum_{i=0}^{m-1} (\phi_i \phi_{m-1-i}''' + \phi_i' \phi_{m-i-i}'') \\ &\quad + \frac{1}{2}\beta_t(t)(3\phi_{m-1}'' + \eta\phi_{m-1}''') - \beta(t)\phi_{t\ m-1}'', \end{aligned} \tag{A17}$$

where the prime denotes differentiation with respect to η.

By substituting the form of Eq. (A6), the general solution for Eq. (A15) can be extracted. Using $\phi_m^*(\eta,t)$ to denote a particular solution of Eq. (A15), one collects

$$\begin{aligned} \phi_m(\eta,t) &= \chi_m \phi_{m-1}(\eta,t) + \phi_m^*(\eta,t) + C_0^m + C_1^m \eta + C_2^m \eta^2 \\ &\quad + C_3^m \eta^3 \quad (m > 0), \end{aligned} \tag{A18}$$

where C_0^m, C_1^m, C_2^m, and C_3^m can be determined from the boundary conditions in Eq. (A16). After some algebra, one gets

$$\begin{aligned} &C_0^m = -\phi_m^*(0,t), \quad C_1^m = -\phi_m^*(1,t) - C_0^m - C_2^m - C_3^m, \\ &C_2^m = -\tfrac{1}{2}\phi_m^{*\prime\prime}(0,t), \\ &C_3^m = \tfrac{1}{2}[\phi_m^*(1,t) - \phi_m^{*\prime}(1,t) + C_0^m + C_2^m]. \end{aligned} \tag{A19}$$

It can thus be seen that the linear relation (A15) may be solved recursively, one order at a time, for $m=1,2,3,\ldots$. We now recall that, according to the definition (A5) of $\mathcal{L}$, the high-order deformation equation (A15) is linear. Then, following the HAM procedure, a nonlinear PDE, such as Eq. (21), may be transformed into an infinite number of linear ODEs. The present approach guarantees the convergence of the series solution by providing the freedom to select a suitable convergence-control parameter $\hbar$ or to use the homotopy-Padé technique.[28–31]

[1] A. S. Berman, "Laminar flow in channels with porous walls," J. Appl. Phys. **24**, 1232 (1953).
[2] R. M. Terrill, "Laminar flow in a uniformly porous channel," Aeronaut. Q. **15**, 299 (1964).
[3] M. Morduchow, "On laminar flow through a channel or tube with injection: Application of method of averages," Q. J. Mech. Appl. Math. **14**, 361 (1957).
[4] J. F. M. White, B. F. Barfield, and M. J. Goglia, "Laminar flow in a uniformly porous channel," Trans. ASME, J. Appl. Mech. **25**, 613 (1958).
[5] J. R. Sellars, "Laminar flow in channels with porous walls at high suction Reynolds numbers," J. Appl. Phys. **26**, 489 (1955).
[6] G. M. Shrestha, "Singular perturbation problems of laminar flow in a uniformly porous channel in the presence of a transverse magnetic field," Q. J. Mech. Appl. Math. **20**, 233 (1967).
[7] W. A. Robinson, "The existence of multiple solutions for the laminar flow in a uniformly porous channel with suction at both walls," J. Eng. Math. **10**, 23 (1976).
[8] F. M. Skalak and C. Y. Wang, "On the nonunique solutions of laminar flow through a porous tube or channel," SIAM J. Appl. Math. **34**, 535 (1978).
[9] J. F. Brady, "Flow development in a porous channel and tube," Phys. Fluids **27**, 1061 (1984).
[10] L. Durlofsky and J. F. Brady, "The spatial stability of a class of similarity solutions," Phys. Fluids **27**, 1068 (1984).
[11] M. B. Zaturska, P. G. Drazin, and W. H. Banks, "On the flow of a viscous fluid driven along a channel by suction at porous walls," Fluid Dyn. Res. **4**, 151 (1988).
[12] G. I. Taylor, "Fluid flow in regions bounded by porous surfaces," Proc. R. Soc. London, Ser. A **234**, 456 (1956).
[13] S. W. Yuan, "Further investigation of laminar flow in channels with porous walls," J. Appl. Phys. **27**, 267 (1956).
[14] I. Proudman, "An example of steady laminar flow at large Reynolds number," J. Fluid Mech. **9**, 593 (1960).
[15] R. M. Terrill and G. M. Shrestha, "Laminar flow through parallel and uniformly porous walls of different permeability," Z. Angew. Math. Phys. **16**, 470 (1965).
[16] G. M. Shrestha and R. M. Terrill, "Laminar flow with large injection through parallel and uniformly porous walls of different permeability," Q. J. Mech. Appl. Math. **21**, 413 (1968).
[17] J. F. Brady and A. Acrivos, "Steady flow in a channel or tube with an acceleration surface velocity: An exact solution to the Navier–Stokes equations with reverse flow," J. Fluid Mech. **112**, 127 (1981).
[18] E. B. B. Watson, W. H. H. Banks, M. B. Zaturska, and P. G. Drazin, "On transition to chaos in two-dimensional channel flow symmetrically driven by accelerating walls," J. Fluid Mech. **212**, 451 (1990).
[19] P. Watson, W. H. Banks, M. B. Zaturska, and P. G. Drazin, "Laminar channel flow driven by accelerating walls," Eur. J. Appl. Math. **2**, 359 (1991).
[20] E. C. Dauenhauer and J. Majdalani, "Exact self-similarity solution of the Navier–Stokes equations for a porous channel with orthogonally moving walls," Phys. Fluids **15**, 1485 (2003).
[21] J. Majdalani and C. Zhou, "Moderate-to-large injection and suction driven channel flows with expanding or contracting walls," J. Appl. Math. Mech. **83**, 181 (2003).
[22] J. Majdalani, C. Zhou, and C. A. Dawson, "Two-dimensional viscous flow between slowly expanding or contracting walls with weak permeability," J. Biomech. **35**, 1399 (2002).
[23] C. Zhou and J. Majdalani, "Improved mean flow solution for slab rocket motors with regressing walls," J. Propul. Power **18**, 703 (2002).
[24] A. D. MacGillivray and C. Lu, "Asymptotic solution of a laminar flow in a porous channel with large suction: A nonlinear turning point problem," Methods Appl. Anal. **1**, 229 (1994).
[25] C. Lu, A. D. MacGillivray, and S. P. Hastings, "Asymptotic behaviour of solutions of a similarity equation for laminar flows in channels with porous walls," IMA J. Appl. Math. **49**, 139 (1992).
[26] S. M. Cox and A. C. King, "On the asymptotic solution of a high-order nonlinear ordinary differential equation," Proc. R. Soc. London, Ser. A **453**, 711 (1997).
[27] S. Liao, "Notes on the homotopy analysis method: Some definitions and theorems," Commun. Nonlinear Sci. Numer. Simul. **14**, 983 (2009).
[28] S. Liao, "A kind of approximate solution technique which does not depend upon small parameters—II. An application in fluid mechanics," Int. J. Non-Linear Mech. **32**, 815 (1997).
[29] S. Liao, *Beyond Perturbation: Introduction to the Homotopy Analysis Method* (Chapman and Hall, London/CRC, Boca Raton, FL, 2003).
[30] S. Liao, "A general approach to obtain series solutions of nonlinear differential equations," Stud. Appl. Math. **119**, 297 (2007).
[31] S. Liao, "On the homotopy analysis method for nonlinear problems," Appl. Math. Comput. **147**, 499 (2004).

[32]H. Xu, S. J. Liao, and I. Pop, "Series solution of unsteady boundary layer flows of non-Newtonian fluids near a forward stagnation point," J. Non-Newtonian Fluid Mech. **139**, 31 (2006).
[33]H. Xu, S. J. Liao, and I. Pop, "Series solutions of unsteady three-dimensional MHD flow and heat transfer in the boundary layer over an impulsively stretching plate," Eur. J. Mech. B/Fluids **26**, 15 (2007).
[34]S. Abbasbandy, "The application of the homotopy analysis method to nonlinear equations arising in heat transfer," Phys. Lett. A **360**, 109 (2006).
[35]K. Yabushita, M. Yamashita, and K. Tsuboi, "An analytic solution of projectile motion with the quadratic resistance law using the homotopy analysis method," J. Phys. A: Math. Theor. **40**, 8403 (2007).
[36]H. Song and L. Tao, "Homotopy analysis of 1d unsteady, nonlinear groundwater flow through porous media," J. Coastal Res. **50**, 292 (2007).
[37]T. Hayat and M. Sajid, "Homotopy analysis of MHD boundary layer flow of an upper-convected Maxwell fluid," Int. J. Eng. Sci. **45**, 393 (2007).
[38]F. Allan, "Derivation of the Adomian decomposition method using the homotopy analysis method," Appl. Math. Comput. **190**, 6 (2007).
[39]Y. Wu and K. Cheung, "Explicit solution to the exact Riemann problems and application in nonlinear shallow water equations," Int. J. Numer. Methods Fluids **57**, 1649 (2008).
[40]F. White, *Viscous Fluid Flow* (McGraw-Hill, New York, 1991), pp. 135–136.
[41]S. Liao, "A general approach to get series solution of non-similarity boundary layer flows," Commun. Nonlinear Sci. Numer. Simul. **14**, 2144 (2009).
[42]C. Lu, "On the asymptotic solution of laminar channel flow with large suction," SIAM J. Math. Anal. **28**, 1113 (1997).